creative commons
COMMONS DEED

저작자표시-비영리-변경금지 2.0 대한민국

이용자는 아래의 조건을 따르는 경우에 한하여 자유롭게

- 이 저작물을 복제, 배포, 전송, 전시, 공연 및 방송할 수 있습니다.

다음과 같은 조건을 따라야 합니다:

저작자표시. 귀하는 원저작자를 표시하여야 합니다.

비영리. 귀하는 이 저작물을 영리 목적으로 이용할 수 없습니다.

변경금지. 귀하는 이 저작물을 개작, 변형 또는 가공할 수 없습니다.

- 귀하는, 이 저작물의 재이용이나 배포의 경우, 이 저작물에 적용된 이용허락조건을 명확하게 나타내어야 합니다.
- 저작권자로부터 별도의 허가를 받으면 이러한 조건들은 적용되지 않습니다.

저작권법에 따른 이용자의 권리는 위의 내용에 의하여 영향을 받지 않습니다.

이것은 이용허락규약(Legal Code)을 이해하기 쉽게 요약한 것입니다.

Disclaimer

dCollection

[UCI]I804:24011-200000263950

2013년 8월

석사학위 논문

Fractal dimension analysis of breast cancer cell morphology based on optical imaging

조선대학교 대학원

해양생명과학과

Pham Thi Thuy Linh

Fractal dimension analysis of breast cancer cell morphology based on optical imaging

광학영상 기반 프랙탈 차원 분석을 통한 유방암세포의 형태적 특성 연구

2013년 08월 23일

조선대학교 대학원

해양생명과학과

Pham Thi Thuy Linh

Fractal dimension analysis of breast cancer cell morphology based on optical imaging

지도교수 이 건 호

이 논문을 이학석사학위 신청 논문으로 제출함

2013 년 04 월

조선대학교 대학원

해양생명과학과

Pham Thi Thuy Linh

Pham Thi Thuy Linh 의 석사학위 논문을 인준함

위원장 조선대학교 교 수 이 정 섭 (인)

위 원 조선대학교 부교수 윤 성 명 (인)

위 원 조선대학교 조교수 이 건 호 (인)

2013 년 05 월

조선대학교 대학원

Fractal dimension analysis of breast cancer cell morphology based on optical imaging

A thesis submitted in partial fulfillment

of the requirements for the degree of

Master of Science

by

Pham Thi Thuy Linh

Department of Marine Life Science, Graduate School,

Chosun University, Qwangju, Republic of Korea

2013.05

Approved by:

Prof. Jung Sup Lee, Ph.D. _____

Prof. Seong Myeong Yoon, Ph. D. _____

Major Advisor

Prof. Kun Ho Lee, Ph.D. _____

Contents

List of Figures..... iii

List of Tables..... iv

ABBREVIATIONS..... v

ABSTRACT vi

국문 초록 vi

Chapter 1: Introduction..... 1

Chapter 2: Materials and Methods 5

2.1. Materials..... 5

2.2. Cell culture..... 5

2.3. Atomic force microscope (AFM) imaging 5

2.4. Differential interference contrast (DIC) imaging 6

2.5. Calculation of fractal dimension by box-counting method..... 7

2.6. Statistical analysis..... 9

Chapter 3: Results 10

3.1. Fractal nature of cell boundary structure..... 10

3.2. The molecular basis of the fractal nature of cell boundary ultrastructure..... 14

3.3. Comparison of fractal dimension between normal and cancer cells using AFM imaging..... 18

3.4. Optical imaging is a useful approach to reveal expanding boundary of the cell . 21

3.5. Optimization of high resolution optical imaging for fractal dimension analysis... 24

3.6. Development of FD analysis software for the optical (DIC) image of cells..... 28

3.7. Fractal dimension analysis of breast cancer cell morphology using optical imaging..... 36

3.8. Comparison of fractal dimension between normal, weakly and highly invasive cancer cells using optical imaging..... 42

Chapter 4: Discussion and Conclusion 46

Chapter 5: References..... 49

ACKNOWLEDGMENT 54

List of Figures

Figure 1. Box-counting method for fractal dimension calculation. 8

Figure 2. The cell boundary ultrastructure of MCF10A and its fractal properties. 12

Figure 3. Effect of cytochalasin D treatment on the FD of the MCF10A cell boundary. 16

Figure 4. Comparison between normal and cancer cells using AFM technique. 19

Figure 5. The cell morphologies of different cell lines were captured with (A) atomic force microscope and (B) differential interference contrast microscope.. 22

Figure 6. Optimization of experimental conditions with MDA-MB-231 cell line. 26

Figure 7. Fractal dimension analysis of weakly invasive cancer cell morphology (MCF7, T47D, ZR-75-1) using optical imaging. 37

Figure 8. Fractal dimension analysis of highly invasive cancer cell morphology (MDA-MB-231, MDA-MB-435S, Hs578T) using optical imaging. 39

Figure 9. Comparison between normal, weakly invasive and highly invasive cancer cells using optical imaging. 43

List of Tables

Table 1. Fractal dimension analysis software data of normal cell MCF10A. 29

Table 2. Fractal dimension analysis software data of weakly invasive cancer cell MCF7..... .30

Table 3. Fractal dimension analysis software data of weakly invasive cancer cell T47D. 31

Table 4. Fractal dimension analysis software data of weakly invasive cancer cell ZR-75-1..... 32

Table 5. Fractal dimension analysis software data of highly invasive cancer cell MDA-MB-231 33

Table 6. Fractal dimension analysis software data of highly invasive cancer cell MDA-MB-435S 34

Table 7. Fractal dimension analysis software data of highly invasive cancer cell Hs578T 35

Table 8. Fractal dimension values of individual cells of each cell line..... 41

Table 9. Fractal dimension values of weakly and highly invasive cancer cells..... 45

ABBREVIATIONS

AFM	Atomic force microscope
DIC	Differential interference contrast
DMEM	Dulbecco's Modified Eagle Media
FD	Fractal dimension
KCLB	Korean Cell Line Bank
MEGM	Mammary Epithelial Growth Medium
SD	Standard deviation

ABSTRACT

Fractal dimension analysis of breast cancer cell morphology based on optical imaging

Pham Thi Thuy Linh

Advisor: Prof. Kun Ho Lee, Ph.D.

Department of Marine Life Science,

Graduate School of Chosun University

Fractal geometry is a useful tool for characterizing irregular shapes and complex structures of many natural objects. It allows user-independent evaluation and does not rely on the experience level of the examiner. Recently, fractal dimension has gained increasing applications to analyze biological structures, cellular phenomena and also cancer research. Previous studies of fractal dimension analysis applied to cancer focused on vascular architecture, tumor border and cellular/nuclear morphology. In this study, the fractal property of human MCF10A epithelial cells was explored using atomic force microscope. Treatment with cytochalasin D decreased both the ruggedness and fractal dimension of the cell boundary. Furthermore, fractal property of cell morphology was examined in several breast cancer cell lines with weakly (MCF7, T47D, ZR-75-1), highly (MDA-MB-231,

MDA-MB-435S, Hs578T) invasive potential, and normal cell line (MCF10A) in a comparative approach. The optical imaging of cell membranes of about 20 cells was used for statistical analysis, in which the fractal dimension values of cell boundary were determined by box-counting method. The results showed that the fractal dimensions of the cell boundary decreased when the degree of invasiveness increased. The normal cells (MCF10A) showed the highest fractal dimension value (FD = 1.348), while the weakly invasive cancer cells exhibited the lower fractal dimension value (FD = 1.116 for MCF7, 1.100 for T47D, 1.138 for ZR-75-1) and the highly invasive cancer cells have the lowest fractal dimension value (FD = 1.067 for MDA-MB-231, 1.067 for MDA-MB-435S, 1.079 for Hs578T). There were significant differences of fractal dimension between normal cells and cancer cells, especially between weakly and highly invasive cancer groups as shown by the analysis of variance ($p < 0.05$). Taken together, fractal dimension is a valuable tool to describe irregularity of cell membranes and provides a new way to detect cancer invasiveness stage.

국문 초록

광학영상 기반 프랙탈 차원 분석을 통한 유방암세포의 형태적 특성연구

프랙탈 기하학은 불규칙적인 모양과 복잡한 구조를 갖는, 자연계에 존재하는 많은 사물의 특징을 파악하는데 유용한 도구이다. 프랙탈 기하학은 연구자의 경험과 숙련 수준에 의존하지 않고, 연구자마다 각각 다른 독립적인 평가를 가능하게 한다. 최근, 프랙탈 차원분석은 생물학적인 구조, 세포 현상을 분석하고 또한, 암 연구에 많이 응용되고 있다. 본 연구에서는, 인간의 상피세포 MCF10A의 프랙탈 특성을 원자간력 현미경을 이용하여 분석하였다. 사이토칼라신 D의 처리는 세포 가장자리의 울퉁불퉁함과 프랙탈의 수치를 감소시켰다. 더구나, 세포 형태의 프랙탈적 특성을 몇몇의 유방암 세포주에서 조사하였다. 유방암 세포주는 침입성이 약한 세포주 (MCF7, T47D, ZR-75-1), 침입성이 높은 세포주 (MDA-MB-231, MDA-MB-435S, Hs578T) 를 이용하여, 정상 세포주 (MCF10A) 와 비교 분석하였다. 박스 카운팅으로 구해진 세포 가장자리의 프랙탈 수치를 통계학적으로 분석하는데 약 20가지 세포 세포막의 광학적 이미지를 사용하였다. 실험결과, 세포 가장자리의 프랙탈 수치는 세포의 침입성이 높을수록 감소하였다. 정상 세포주 (MCF10A) 는 가장 높은 프랙탈 수치 (FD = 1.348) 가 나왔고, 침입성이 약한 세포주 (MCF7의 FD = 1.116, T47D의 FD = 1.100, ZR-75-1의 FD = 1.138) 는 더 낮은 수치, 그리고 침입성이 높은 세포주 (MDA-MB-231의 FD = 1.067, MDA-MB-435S의 FD = 1.067, Hs578T의 FD =

1.079) 는 가장 낮게 나왔다. 변화 분석을 통해 보여준 프랙탈 수치 ($p < 0.05$) 에서 정상 세포와 암세포의 차이와 특히, 암세포의 침입성이 낮은 세포와 높은 세포의 차이는 주목할 만한 가치가 있다. 프랙탈 차원분석은 세포막 형태의 불규칙성을 설명하는데 굉장히 유용한 방법이며, 암세포 침입 단계를 알아내는데 새로운 방법을 제공하는 가치있는 도구이다.

Chapter 1: Introduction

Nowadays, cancer is one of the biggest challenges in human society. There are increasing investigations in scientific and clinical research to prevent and cure it. Depending on the abnormal proliferation of cells, a tumor can be benign or malignant. A malignant tumor can invade surrounding normal tissue and spread throughout the body via the circulatory or lymphatic systems (metastasis). One important issue in cancer pathology is determining the cancer stage, especially when the tumor starts invasion and metastasis. But in current situation, most cancer diagnosis is still done by visual examination of specimens in microscope, direct observation of tissues, and so on, which depend on experiences and skills of clinicians a lot (Baish and Jain, 2000). This leads us to the question: how to determine cancer disease stage more precisely and quantitatively.

Before begin the discussion and application of cancer, some background of fractal dimension is necessary. Fractal geometry, first introduced by Benoid Mandelbrot (Mandelbrot, 1982), have been regarded as a powerful tool for describing complex and irregular shapes that cannot be described by classical Euclidian geometry, which is based on smooth shapes such as lines, planes, cylinders and spheres. According to his study, many natural objects such as coastlines (Mandelbrot, 1967), snowflakes, clouds, and mountains have patterns that repeat themselves at different magnifications. This property had been referred to as “statistical self-similarity”. At that case, the degree of complexity and irregularity

can be described by a mathematical value, referred to as fractal dimension. For better understanding about fractal dimension, let's have a look back to traditional Euclidian geometry, where dimension is 1 for a line, 2 for a surface and 3 for a solid. But in natural objects, the fractal dimension does not need to be an integer. For example, the outlines of objects in a two-dimensional image have fractal dimension values between 1 and 2 (Liu *et al.*, 2003), and more complex outlines tend to possess fractal dimension values closer to 2 than 1. With an outlined object in a plane, some methods to measure fractal dimension are available, such as length-related and mass-related method (Smith *et al.*, 1996). Box-counting method is one of the most common methods for calculate fractal dimension, which measures the space-filling behavior of a given object (Song *et al.*, 2005).

Fractal analysis had recently been applied to study a wide range of objects in biology and medicine. It had been used successfully in quantifying many biological structures, such as organs, tissues (Boser *et al.*, 2005; Masters, 2004), and cultured cells (Vilela *et al.*, 1995), even in nuclei and chromatins (Lebedev *et al.*, 2005). With complex morphology of living cells, fractal analysis is especially successful in quantifying brain cell morphologies, such as glial cells and oligodendrocytes (Bernard *et al.*, 2001; Karperien *et al.*, 2013). As discussed above, despite many years of research, a method to precisely and quantitatively determine cancer disease state remains elusive. Because complexity is one of the principal characteristics of biological systems, the measurement of complexity may provide the way to change

this situation for better solutions (Spillman *et al.*, 2004). During the past years, fractal dimension has gained increasing applications in tumor pathology (Di Giovanni *et al.*, 2012; Omori *et al.*, 2002). Some growing studies show fractals to be useful measures of the pathologies of the vascular architecture, tumor/parenchymal border, and cellular/nuclear morphology. Fractal measures were used to characterize the microvasculature in cutaneous melanoma (Heymans *et al.*, 1999). In other study, the epithelial–connective tissue interface of the oral musaco was examined (Landini and Rippin, 1996).

Besides applications of fractal analysis to tumor vasculature and tumor border, some groups are seeking to extend the use of fractals to abnormalities of cellular and nuclear structures. Nuclear fractal dimension was examined in oral squamous cell carcinoma (Goutzanis *et al.*, 2008), nuclear heterochromatin structure of MCF7 combined with plasma membrane enzyme (Losa *et al.*, 1998), or fractal analysis was used to identifying atypical nuclei in dysplastic lesions of the cervix uteri (Sedivy *et al.*, 1999). Notably, some cancer invasion research started to form with fractal dimension (Ahammera, 2001; 2008).

Therefore, exploring the fractal property of cancer cell morphology may give valuable information and approach in cancer research. In this study, the characteristics of cell morphology were investigated and visualized in many breast cancer cell lines, and normal cell line (MCF10A) in a comparative approach. In next step, the geometric complexity of cell boundaries was investigated by fractal

analysis. The picture of cell morphology were taken by differential interference contrast (DIC) microscope which produces impressive 3D-like images of unstained specimens with high resolution. The box-counting method was used to calculate fractal dimension value.

Chapter 2: Materials and Methods

2.1. Materials

The breast cancer cell lines were obtained from Korean Cell Line Bank (KCLB), the culture medium from GIBCO, cholera toxin, bovine insulin, and gelatin were from Sigma. The list of cell lines can be divided into 3 groups: normal cell (MCF10A), weakly invasive cancer cells (MCF7, T47D, ZR-75-1) and highly invasive cancer cells (MDA-MB-231, MDA-MB-435S, Hs578T).

2.2. Cell culture

All cells were cultured at 37°C in a humidified incubator equilibrated with 95% air/5% CO_2. All culture conditions and procedures follow the KCLB recommendations. The normal cells (MCF10A) were cultured in Mammary Epithelial Growth Medium (MEGM, Clonetics) supplemented with 100 ng/ml cholera toxin (Sigma). MCF7 cells were cultured in Dulbecco's modified Eagle media (DMEM, GIBCO) supplemented with 10% fetal bovine serum (HyClone) and 0.01 mg/ml bovine insulin (Sigma). MDA-MB-435S, Hs578T cells were cultured in Dulbecco's modified Eagle media (DMEM, GIBCO) supplemented with 10% fetal bovine serum (HyClone). T47D, ZR-75-1, MDA-MB-231 cells were cultured in RPMI-1640 (GIBCO) supplemented with 10% fetal bovine serum (HyClone).

2.3. Atomic force microscope (AFM) imaging

For AFM imaging in an aqueous environment, cells were cultured for 24 hr in 35-mm dishes and fixed with freshly prepared 4% paraformaldehyde for 10 min. For dual imaging of the identical region of a cell with AFM and optical microscopy, cells were cultured on a coverslip with a grid of 55 μm squares (Eppendorf). All AFM analyses of cells were conducted in phosphate buffered saline using an AFM system (XE-100, Park Systems) with a sharpened square pyramid-shaped 120 μm AFM cantilever (HYDRA-G, Applied Nanostructures). The spring constant and resonance frequency of the cantilever were 0.60 N/m and 54 kHz, respectively. The total signal on the AFM photo detector was set at 2~3 V, and the scan rate was set at approximately 0.4 Hz to optimize image quality. All AFM images including topography and error signal image were collected in contact mode at 30 x 30 μm^2 measured area with a resolution of 512 x 512 pixels.

2.4. Differential interference contrast (DIC) imaging

This study used No.1 glass coverslips (Marienfeld) to have optimal microscopic images. For coating coverslips, the coverslips were incubated with 0.2% gelatin in distilled water for 1 hr and dried at room temperature for 1 hr prior to use. To prepare samples for DIC microscope, cells were plated on coverslips at a concentration of about 10^5 cells per 35 mm culture dish. Cells were cultured for 24 hr to have well-spreading cell membrane and fixed with 3.7% paraformaldehyde for 15 min. The coverslips were then mounted with mounting oil (Dako). All samples were stored at 4°C and observed under microscope within 24 hr. All DIC images of

cells were captured by Olympus Fluoview 1000 unit with IX81 motorized inverted microscope. Cells were observed with high resolution 60X oil objective lens (UPLSAPO, NA = 1.35) and focused on cell membrane of a single cell. The original images were collected at 4000X magnification at OIB format of 1024 × 1024 pixels and export to TIFF file for further analysis. Each cell line was taken about 20 high quality images for statistical analysis.

2.5. Calculation of fractal dimension by box-counting method

One of the most common methods to measure fractal dimension in biological science is box-counting method (Cross, 1997). Boxes of varying sizes are applied to the outline and the number of outline containing squares is counted (Fig. 1). The formula for the box-counting dimension is given by

$$FD = \lim_{L \to 0} \frac{\mathrm{Log}\, N}{\mathrm{Log}\, 1/L}$$

where FD is the box-counting fractal dimension of the object, L is the side length of the box, and N is the smallest number of boxes of side length L required to cover completely the outline of the object being measured. However, the limit zero cannot be applied to biological objects, so an empirical equation can be given by

$$FD = d$$

where d is the slope of the graph of the log N against log1/L. It can be seen that the box size gets smaller, the results become more detailed and accurate.

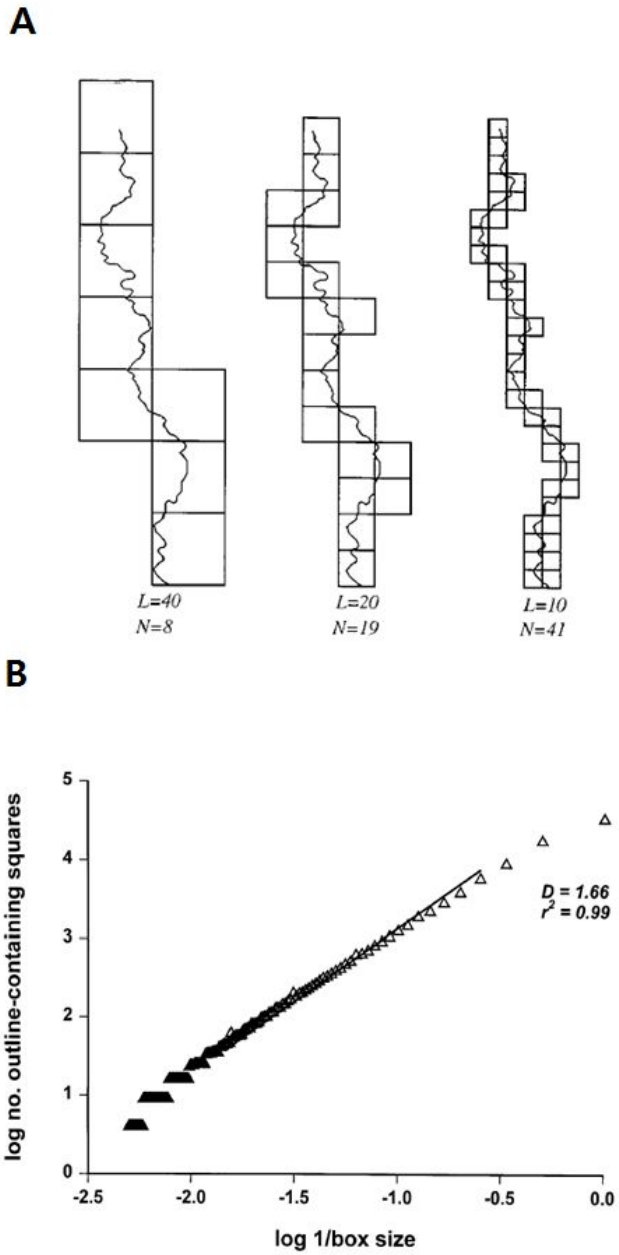

Figure 1. Box-counting method for fractal dimension calculation. (A) The image covered by boxes of decreasing size. (B) Best fit of number of boxes to size of boxes.

2.6. Statistical analysis

Data were expressed as mean ± SD of independent cells. For comparison of fractal dimension values between groups, data were analyzed by single factor ANOVA (Microsoft Excel). A value of $p < 0.05$ was considered statistically significant.

Chapter 3: Results

3.1. Fractal nature of cell boundary structure

In order to access the geometry complexity of breast epithelial cell boundary, an image of MCF10A single cell was first obtained from atomic force microscope (AFM). From the image, cell boundaries were extracted and the fractal dimensions of individual objects were measured (Figs. 2A and 2B). After eliminating background noise, the gray scale images were converted to binary form by selecting a suitable threshold, allowing the conservation of most of the finest processes of the cell (Fig. 2C). Finally, the contours of the cell boundary were acquired by a discrete wavelet transform algorithm and subjected to fractal analysis (Fig. 2D). The box-counting method was used to determine the FD value of a typical leading edge image of a MCF10A cell. The FD was calculated from the slope of the linear regression of the log of the number of occupied boxes against the log of the corresponding box size as described in Materials and Methods. The high value of the correlation coefficient of the linear regression of the log/log plot ($r \geq 0.995$) shows that the irregularity of the cell boundary remains constant over a wide range of magnifications; notably, this property is the defining characteristic of fractal objects. Fractal analysis by the box-counting method is a useful approach for quantifying the complexity of the cell boundary nanostructure (Figs.2E-2G).

Therefore, the self-similarity property of the cell boundary was also examined by comparing the fractal dimensions calculated from the entire image with those

calculated from smaller parts of the same image (Figs. 2E-2G). The resulting FD values were almost identical thus confirming the fractal nature of the leading edge of MCF10A cells.

Figure 2. The cell boundary ultrastructure of MCF10A and its fractal properties. (A) The original AFM error signal image. (B) Image after the histogram distribution, smoothing, and thresholding procedures. (C) Image after the noise filtering process and binary transformation. (D) Outlined cell contour line. (E-G) Fractal dimensions of the entire boundary line (E) and the upper-left part of (E) is shown in (F), the lower-right is shown in (G). The two calculated FD values in (F) and (G) are similar to the entire boundary line in (E). This implies that boundary structure of MCF10A cells exhibits self-similarity in its geometric boundary.

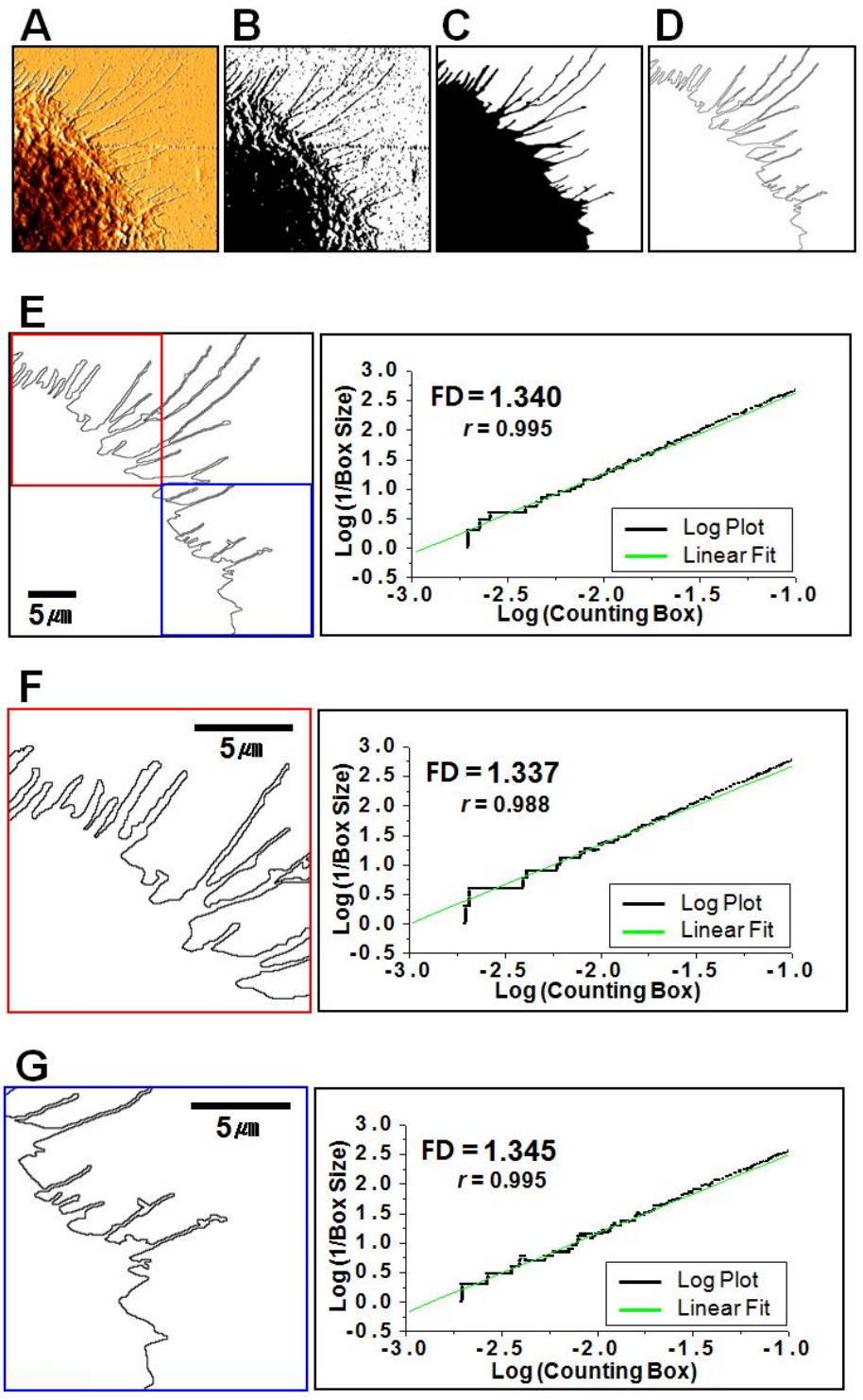
A
B
C
D
E
5 μm
FD = 1.340
r = 0.995
Log (1/Box Size)
Log (Counting Box)
Log Plot
Linear Fit
F
5 μm
FD = 1.337
r = 0.988
Log (1/Box Size)
Log (Counting Box)
Log Plot
Linear Fit
G
5 μm
FD = 1.345
r = 0.995
Log (1/Box Size)
Log (Counting Box)
Log Plot
Linear Fit

3.2. The molecular basis of the fractal nature of cell boundary ultrastructure

The magnitude of the FD of the cell boundary is weighted by the ruggedness of the plasma membrane, which is mainly affected by the two distinct actin-based membrane protrusions, filopodia and lamellipodia. These highly dynamic structures are intimately linked to the turnover of actin filaments and function in a variety of cellular processes including migration, wound healing and neurite outgrowth, depending on the cell type (Mattila and Lappalainen, 2008). The underlying uniformity of actin dynamics may provide an explanation for the relative constancy of the fractal dimension despite the morphological irregularity of individual MCF10A cells. To test this hypothesis, cells were treated with cytochalasin D (1 μM), a fungal drug that causes depolymerization and disruption of actin filaments, and imaged after different exposure times to the drug. After 30 min of drug treatment, filopodia were markedly retracted and degraded (Fig. 3A). Over time, this effect became more evident and was almost maximal at 2 hr. However, AFM imaging revealed only minor alterations of the lamellipodia-like structures in response to cytochalasin D. Therefore, the fractal dimensions of the cell borders were examined at the indicated times (Fig. 3B). The mean FD value gradually decreased up to 1 hr after cytochalasin D treatment, although the individual levels somewhat fluctuated. The effect appeared to level off after 2 hrs of drug treatment, with no significant individual variations in FD (Fig. 3B and data not shown). Taken together, these results suggest that differences in FD values of the cell boundary ultrastucture are largely due to the

degree of integrity and dynamics of the actin filaments abutting the plasma membrane. This finding implies that FD may be a useful parameter for assessing not only the morphological complexity of a given cell type, but also the exuberance of its actin-based membrane protrusions, especially filopodia.

Figure 3. Effect of cytochalasin D treatment on the FD of the MCF10A cell boundary. (A) Representative AFM images of cytochalasin D-treated MCF10A cells after 0, 30, 60 and 120 min of exposure to cytochalasin D. Over time, the filopodia become more contracted and dispersed. (B) Statistical plot of FD (mean ± S.E.) with respect to time after cytochalasin D treatment. The FD value declines with time, and its magnitude is mainly influenced by the integrity of the intracellular actin cytoskeleton.

A

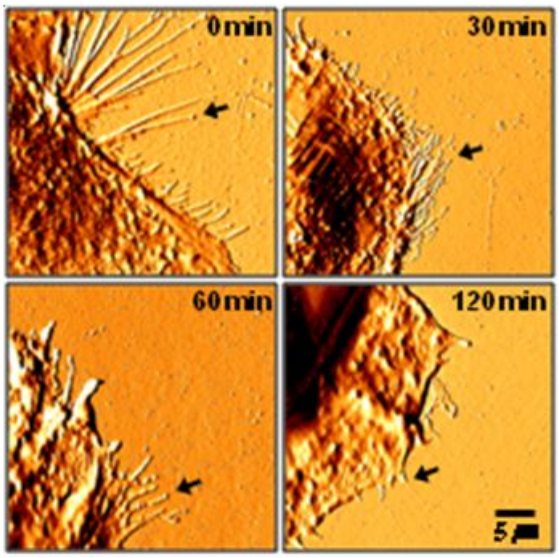
0 min
30 min
60 min
120 min
5 μm

B

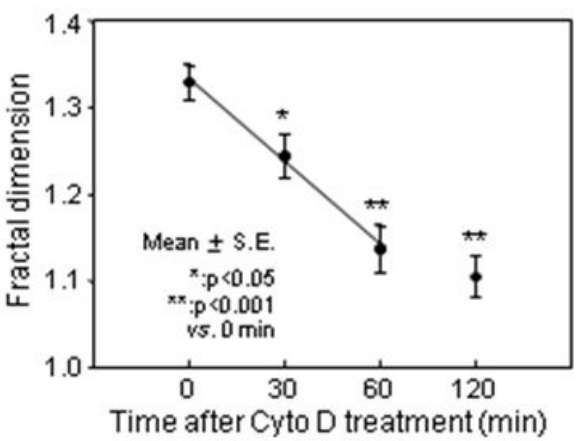
Fractal dimension
1.4
1.3
1.2
1.1
1.0
Mean ± S.E.
*:p<0.05
**:p<0.001
vs. 0 min
*
**
**
0
30
60
120
Time after Cyto D treatment (min)

3.3. Comparison of fractal dimension between normal and cancer cells using AFM imaging

Atomic force microscopy (AFM) is a valuable tool for exploring the surface ultrastructure of biological materials, including macromolecular ensembles and the plasma membrane of cells. Determination of fractal dimension by box-counting method is possible to derive a quantitative measure for the raggedness of cells or small biological organisms. With this method, the fractal dimension analysis was investigated on some different cell lines: MCF10A (normal cell), MCF7 (weakly invasive cancer cell) and MDA-MB-231 (highly invasive cancer cell) (Fig. 4). About 10 AFM images of each cell line were processed and calculated fractal dimension value by box-counting method.

The results showed that there is difference between normal cells, weakly invasive cancer cells and highly invasive cancer cells which implies in both cellular morphology and fractal dimension value. The high resolution images of MCF10A show more complexity in membranes and have higher fractal dimension value (FD = 1.231 ± 0.042), while cell membranes of MCF7 show less branching and have lower fractal dimension values (FD = 1.081 ± 0.007), the MDA-MB-231 cells show rather smooth membranes and have lowest fractal dimension values (FD = 1.040 ± 0.005).

Figure 4. Comparison between normal and cancer cells using AFM technique. (A) The cell morphologies of normal cells MCF10A, weakly invasive cancer cells MCF7 and highly invasive cancer cells MDA-MB-231 were collected by AFM technique. These structures were clearly different between normal cells and cancer cells. (B) Fractal dimension values of normal cells MCF10A, weakly invasive cancer cells MCF7 and highly invasive cancer cells MDA-MB-231. The fractal dimension values clearly decreased from 1.231 ± 0.042 in normal cells to 1.081 ± 0.007 in weekly invasive cancer cells and 1.040 ± 0.005 in highly invasive cancer cells, gave that fractal dimension was useful morphological descriptor in establishing links between structure and function.

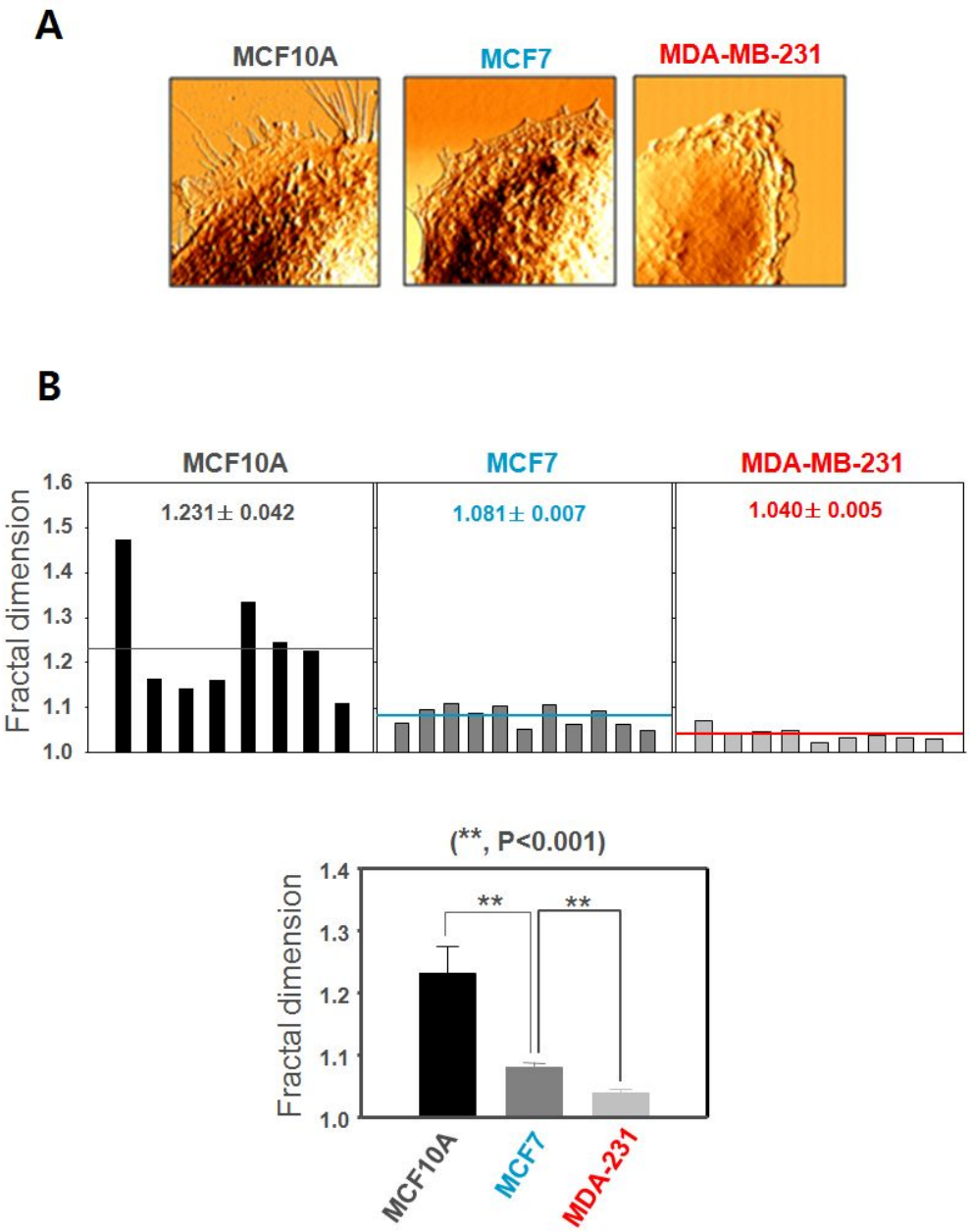
A
MCF10A
MCF7
MDA-MB-231
B
MCF10A
MCF7
MDA-MB-231
1.231± 0.042
1.081± 0.007
1.040± 0.005
Fractal dimension
1.6
1.5
1.4
1.3
1.2
1.1
1.0
(**, P<0.001)
**
**
Fractal dimension
1.4
1.3
1.2
1.1
1.0
MCF10A
MCF7
MDA-231

3.4. Optical imaging is a useful approach to reveal expanding boundary of the cell

The AFM images showed that there was difference of fractal dimension between MCF10A, MCF7, MDA-MB-231. To test this difference really exists between normal cell, weakly invasive and highly invasive cancer cells, it is necessary to extend fractal analysis of other cell lines and obtain more FD values in each cell line. AFM technique visualizes the fine structures of the cell boundaries. But when fractal analysis is measured with a large cell number, AFM technique has big disadvantage when it has a little complex procedure and takes long time to have one high quality image. It is essential to seek a more useful and faster method to visualize cell boundary structure.

Therefore, another different imaging technique was tested, optical imaging [in this case differential interference contrast microscope (DIC)]. The pictures of AFM and DIC with different cell lines are shown in Fig. 5. It can be seen that AFM images have better quality but DIC imaging can also collect precise and fine cell membrane structure, especially the profuseness of branching and the ruggedness of the border (Fig. 5). Furthermore, with optical imaging, a large cell sample can be screened in the short time and the collected data can be analyzed statistically. It gives more accurate information when difference from cell to cell is reduced. On the other hand, experiment procedures become simple and fractal dimension analysis can be processed with many cell lines. Indeed, these advantages will be proved in the following results.

Figure 5. The cell morphologies of different cell lines were captured with (A) atomic force microscope and (B) differential interference contrast microscope. The images were taken with MCF10A, MCF7, MDA-MB-231 cell lines. There was no significant difference between atomic force microscope (AFM) images and differential interference contrast (DIC) images. Both techniques can collect the clear cell membrane. Because the DIC technique was more simple and faster, it was selected to study cell morphology and fractal dimension analysis.

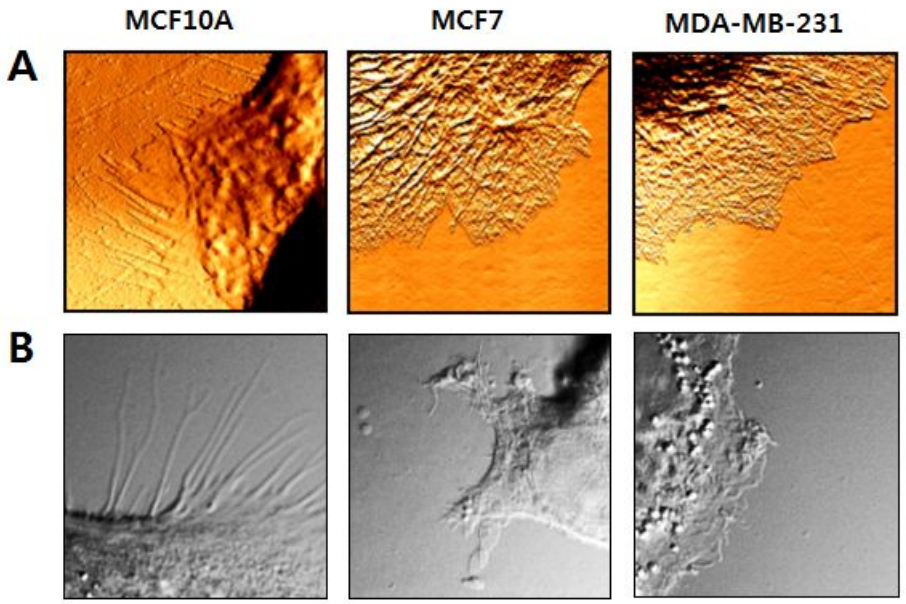
MCF10A
MCF7
MDA-MB-231
A
B

3.5. Optimization of high resolution optical imaging for fractal dimension analysis

Because the purpose of this study is analyzing fractal property of cell morphology, the more clear and high quality images can be taken, the more exact and believable fractal dimension values are calculated. In normal experimental conditions, it seems to be difficult to get high quality images which can reflect clear characteristic of cellular membrane (Fig. 6C). Therefore, the experimental procedures were optimized to find out the best conditions for optical imaging.

There are many factors which can affect the quality of cell boundary imaging: cell culture condition, culture substrate (coverslip), coverslip coating condition, fixation condition, the quality of objective lens and the light source of microscope. Therefore, independent experiments were performed under various conditions and the quality of cell images was compared. The results of every experiment were shown in Fig. 6.

All cell lines were maintained in very good condition during experimental period. The cells were cultured with different kinds of coverslip (plastic coverslip, glass coverslip) and different coating condition (gelatin coating, collagen coating). It can be seen that the cells cultured on glass coverslip showed better membrane images than plastic coverslip, and coverslips coated with gelatin solution are better than coverslips coated with collagen (Fig. 6A). Finally, the experimental condition was decided that the cells were cultured on glass coverslip coated with 0.2% gelatin

solution. After fixation with paraformaldehyde, the cells needed to be observed under microscope within 24 hr to avoid the effect of mounting oil to cell membrane in long-term storage (Fig. 6B).

Normally, the low magnification optical imaging cannot reflect the characteristics of cell boundary clearly. In this study, a high magnification system was used to improve optical imaging quality. Every images were taken with 60X oil objective lens of Olympus Fluoview 1000 Confocal Microscope at high magnification (4000X) (Fig. 6C). The quality of images was increased and can collect all cellular membrane characteristics precisely.

Figure 6. Optimization of experimental conditions with MDA-MB-231 cell line. (A) The cells were cultured on different kinds of coverslip (plastic or glass coverslips) and different kinds of coating solution (gelatin or collagen coating). The cells cultured on glass coverslip coated with gelatin showed the best image. (B) The samples were observed under microscope within 1 day better than long time (5 days). (C) Comparison between normal optical imaging and high rosultion optical imaging. The high resolution optical imaging were collected with 60X oil objective lens of Olympus Confocal Microscope and can reflect characteristics of cell membrane clearly.

A

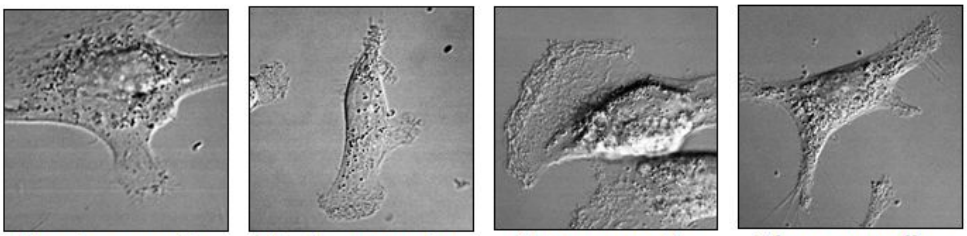

Plastic coverslip
Gelatin coating

Plastic coverslip
Collagen coating

Glass coverslip
Gelatin coating

Glass coverslip
Collagen coating

B

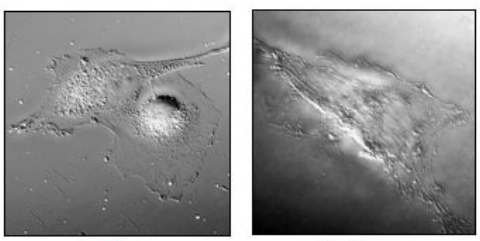

1 day

5 days

C

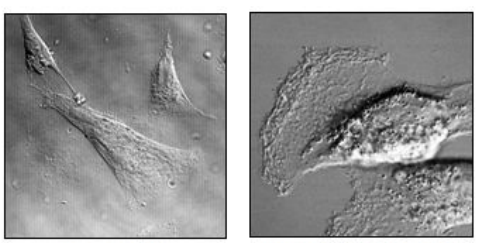

Normal
optical imaging

High resolution
optical imaging

3.6. Development of FD analysis software for the optical (DIC) image of cells

In this study, a software was developed and used to calculate fractal dimension value of cell boundary. The software was developed based on the principle of box-counting method. The software helps fractal dimension analysis more convenient and gives more reliable calculation results.

Firstly, the cell image was loaded into the software. Users can choose one special cell membrane region for calculation FD. In next step, users can reduce box sizes (64, 32, 16, 8 pixels) and mark the boxes which cover the cell boundary. The software will automatically count the number of occupied boxes and compute fractal dimension value from the slope of the linear regression between the log of box number and the log of corresponding boxes' size.

The software was used to calculate FD values of normal cells (MCF10A), weakly invasive cancer cells (MCF7, T47D, ZR-75-1), highly invasive cancer cells (MDA-MB-231, MDA-MB-435S, Hs578T). The results of box number counted with 32 and 16 pixels were shown in Table 1-7. Other data were not shown.

Table 1. Fractal dimension analysis software data of normal cell MCF10A.

Image	Box size (pixels)	Box number	FD	Image	Box size (pixels)	Box number	FD
1	32	32	1.438	11	32	93	1.330
	16	87			16	234	
2	32	98	1.238	12	32	36	1.445
	16	243			16	98	
3	32	60	1.410	13	32	51	1.348
	16	177			16	144	
4	32	96	1.321	14	32	35	1.330
	16	240			16	88	
5	32	28	1.269	15	32	62	1.313
	16	80			16	177	
6	32	60	1.345	16	32	28	1.241
	16	150			16	73	
7	32	40	1.367	17	32	69	1.231
	16	112			16	162	
8	32	80	1.301	18	32	33	1.382
	16	210			16	86	
9	32	34	1.486	19	32	57	1.395
	16	89			16	136	
10	32	49	1.408	20	32	40	1.421
	16	130			16	121	
-	-	-	-	21	32	30	1.283
	-	-			16	73	

Table 2. Fractal dimension analysis software data of weakly invasive cancer cell MCF7.

Image	Box size (pixels)	Box number	FD	Image	Box size (pixels)	Box number	FD
1	32	35	1.029	11	32	55	1.149
	16	81			16	122	
2	32	37	1.180	12	32	51	1.098
	16	84			16	104	
3	32	43	1.170	13	32	36	1.115
	16	97			16	78	
4	32	32	1.252	14	32	48	1.119
	16	70			16	97	
5	32	35	1.180	15	32	34	1.160
	16	74			16	76	
6	32	29	1.092	16	32	40	1.070
	16	57			16	84	
7	32	36	1.134	17	32	58	1.175
	16	79			16	131	
8	32	48	1.079	18	32	39	1.107
	16	106			16	84	
9	32	41	1.069	19	32	50	1.102
	16	86			16	106	
10	32	42	0.929	-	-	-	-
	16	80			-	-	

Table 3. Fractal dimension analysis software data of weakly invasive cancer cell T47D.

Image	Box size (pixels)	Box number	FD	Image	Box size (pixels)	Box number	FD
1	32	27	1.100	11	32	26	1.107
	16	50			16	56	
2	32	27	1.103	12	32	29	1.208
	16	58			16	67	
3	32	51	0.927	13	32	39	0.937
	16	97			16	82	
4	32	27	0.946	14	32	27	1.245
	16	52			16	64	
5	32	36	1.078	15	32	38	1.079
	16	76			16	80	
6	32	32	1.150	16	32	42	1.237
	16	71			16	99	
7	32	44	1.110	17	32	27	1.197
	16	95			16	54	
8	32	37	1.065	18	32	39	1.196
	16	75			16	89	
9	32	45	1.047	-	-	-	-
	16	93			-	-	
10	32	19	1.074	-	-	-	-
	16	40			-	-	

Table 4. Fractal dimension analysis software data of weakly invasive cancer cell ZR-75-1.

Image	Box size (pixels)	Box number	FD	Image	Box size (pixels)	Box number	FD
1	32	34	1.062	12	32	40	1.087
	16	71			16	85	
2	32	18	1.078	13	32	36	1.097
	16	38			16	77	
3	32	54	1.065	14	32	22	1.095
	16	113			16	47	
4	32	57	1.098	15	32	46	1.149
	16	122			16	102	
5	32	24	1.130	16	32	37	1.130
	16	49			16	81	
6	32	28	1.114	17	32	27	1.240
	16	72			16	59	
7	32	34	1.234	18	32	50	1.124
	16	80			16	109	
8	32	23	1.258	19	32	40	1.053
	16	55			16	83	
9	32	27	1.152	20	32	30	1.159
	16	60			16	67	
10	32	40	1.217	21	32	36	1.067
	16	93			16	79	
11	32	39	1.238	22	32	53	1.179
	16	92			16	120	

Table 5. Fractal dimension analysis software data of highly invasive cancer cell MDA-MB-231.

Image	Box size (pixels)	Box number	FD	Image	Box size (pixels)	Box number	FD
1	32	43	1.066	11	32	30	1.070
	16	90			16	63	
2	32	41	1.166	12	32	23	1.031
	16	92			16	47	
3	32	36	1.152	13	32	45	1.078
	16	80			16	95	
4	32	34	1.042	14	32	23	1.095
	16	70			16	51	
5	32	27	0.920	15	32	31	1.103
	16	51			16	68	
6	32	31	1.068	16	32	37	1.060
	16	65			16	77	
7	32	33	1.145	17	32	50	1.080
	16	73			16	96	
8	32	29	1.049	18	32	31	1.052
	16	60			16	62	
9	32	38	1.056	19	32	27	1.002
	16	79			16	54	
10	32	29	1.077	20	32	52	1.028
	16	59			16	106	

Table 6. Fractal dimension analysis software data of highly invasive cancer cell MDA-MB-435S.

Image	Box size (pixels)	Box number	FD	Image	Box size (pixels)	Box number	FD
1	32	44	1.110	11	32	45	1.032
	16	95			16	92	
2	32	30	1.121	12	32	33	0.937
	16	63			16	66	
3	32	28	1.169	13	32	31	0.999
	16	63			16	62	
4	32	31	1.068	14	32	38	1.144
	16	65			16	84	
5	32	36	1.116	15	32	23	1.000
	16	65			16	46	
6	32	33	1.204	16	32	27	0.936
	16	76			16	58	
7	32	27	0.978	17	32	33	0.999
	16	53			16	69	
8	32	39	1.072	18	32	38	1.092
	16	82			16	81	
9	32	38	1.109	19	32	31	1.112
	16	82			16	67	
10	32	22	1.064	20	32	20	1.070
	16	46			16	42	

Table 7. Fractal dimension analysis software data of highly invasive cancer cell Hs578T.

Image	Box size (pixels)	Box number	FD	Image	Box size (pixels)	Box number	FD
1	32	51	1.160	11	32	34	1.042
	16	114			16	70	
2	32	41	0.936	12	32	25	1.084
	16	84			16	53	
3	32	30	1.190	13	32	29	1.096
	16	66			16	62	
4	32	28	1.141	14	32	31	1.068
	16	62			16	65	
5	32	42	1.121	15	32	29	1.115
	16	91			16	58	
6	32	40	1.154	16	32	41	1.102
	16	89			16	80	
7	32	25	1.013	17	32	40	0.999
	16	52			16	80	
8	32	44	1.054	18	32	38	1.109
	16	86			16	82	
9	32	25	1.071	19	32	28	1.051
	16	51			16	58	
10	32		1.014	20	32	39	1.054
	16				16	81	
-	-	-	-	21	32	20	1.094
	-	-			16	40	

3.7. Fractal dimension analysis of breast cancer cell morphology using optical imaging

Based on optical imaging and development of software for fractal analysis, I investigated in weakly invasive (MCF7, T47D, ZR-75-1) and highly invasive (MDA-MB-231, MDA-MB-435S, Hs578T) cancer cells to explore morphological changes during cancer metastasis progression. As control, the normal cells (MCF10A) was processed. All of cell lines are epithelial cells isolated from mammary gland of human female. In each cell lines, about 20 cells were examined and the fractal dimension values were determined. The typical images of cell membrane are shown in Fig. 7 (weakly invasive cancer cell) and Fig. 8 (highly invasive cancer cell). The fractal dimension results of individual cells are shown in Table 8 and calculated with mean ± SD value.

In order to have a clear picture we need to have a deep look at fractal dimension values inside each group. In weakly invasive cancer cells, the fractal dimension of each cell line is close to those of the others (FD = 1.116 for MCF7, 1.100 for T47D and 1.138 for ZR-75-1). Similar observation is obtained with highly invasive cancer cells where the fractal dimension value is 1.067 for MDA-MB-231, 1.067 for MDA-MB-435S and 1.079 for Hs578T. The mean value is 1.118 ± 0.019 for weakly invasive cancer cells (Fig. 7B) and 1.071 ± 0.007 for highly invasive cancer cells (Fig. 8B). Fractal dimension results reveal the relationship between fractal property of cell boundary and invasiveness stage.

Figure 7. Fractal dimension analysis of weakly invasive cancer cell morphology (MCF7, T47D, ZR-75-1) using optical imaging. (A) The typical images were captured from differential interference contrast microscope. Scale bar, 5 μm. Around 20 high quality images of each cell line were taken. (B) Fractal dimension values were calculated by box-counting method. Data were expressed as the mean ± SD values of experiments. The FD value of MCF7 is 1.116 ± 0.069, similar to T47D (1.100 ± 0.097) and ZR-75-1 (1.138 ± 0.065). The calculated FD value for weakly invasive cell group is 1.118 ± 0.019.

A

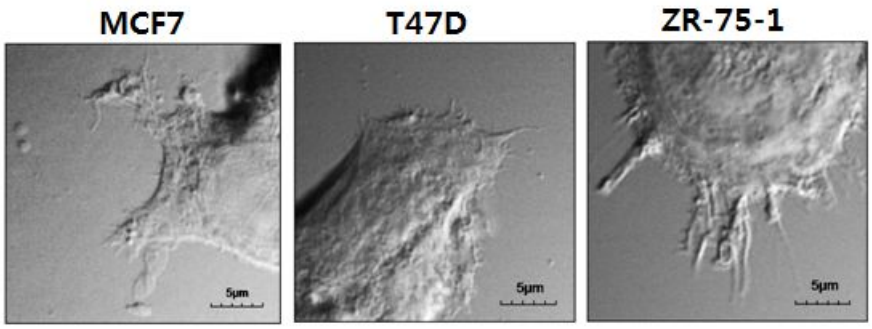
MCF7
T47D
ZR-75-1
5μm
5μm
5μm

B

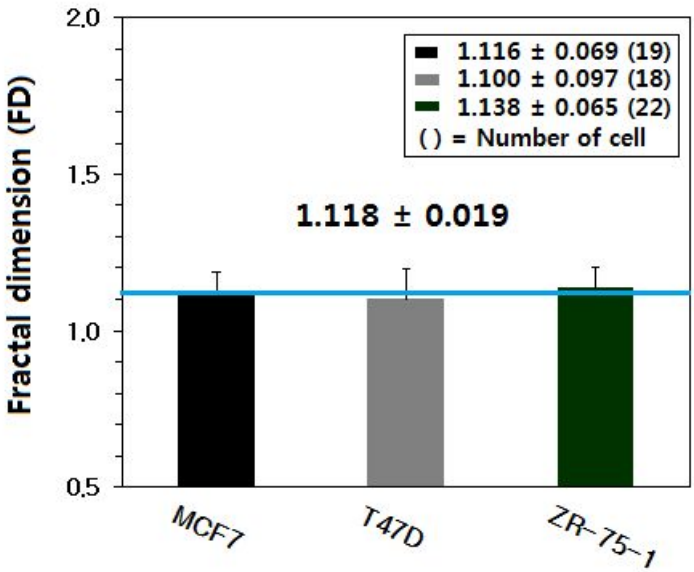
Fractal dimension (FD)
2.0
1.5
1.0
0.5
1.116 ± 0.069 (19)
1.100 ± 0.097 (18)
1.138 ± 0.065 (22)
( ) = Number of cell
1.118 ± 0.019
MCF7
T47D
ZR-75-1

Figure 8. Fractal dimension analysis of highly invasive cancer cell morphology (MDA-MB-231, MDA-MB-435S, Hs578T) using optical imaging. (A) The typical images were captured from differential interference contrast microscope. Scale bar, 5 μm. Around 20 high quality images of each line were taken. (B) Fractal dimension values were calculated by box-counting method. Data were expressed as the mean ± SD values of experiments. The FD value of MDA-MB-231 is 1.067 ± 0.054, similar to MDA-MB-435S (1.067 ± 0.074) and Hs578T (1.079 ± 0.060). The calculated FD value for highly invasive cancer cell group is 1.071 ± 0.007.

A

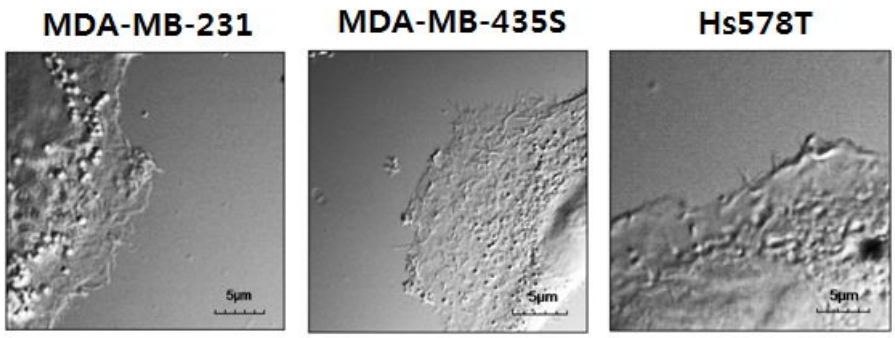
MDA-MB-231
MDA-MB-435S
Hs578T
5μm
5μm
5μm

B

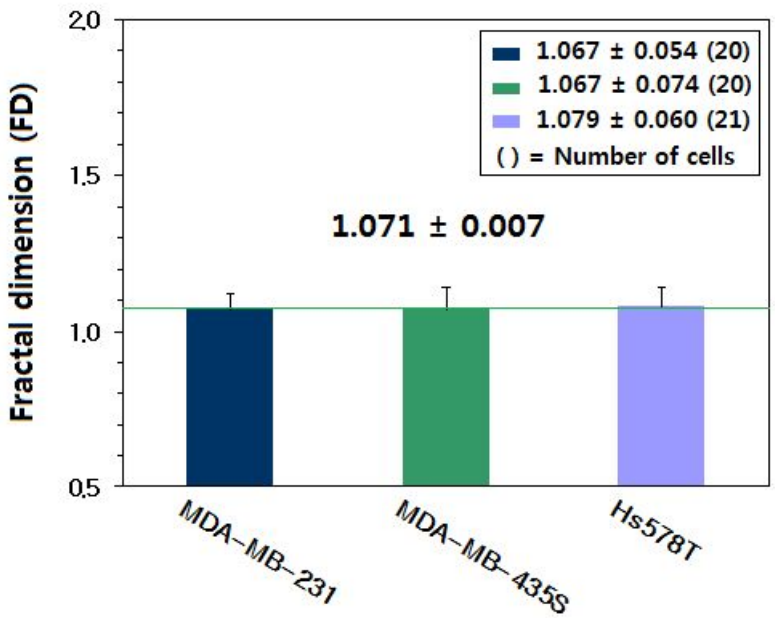
Fractal dimension (FD)
2.0
1.5
1.0
0.5
1.067 ± 0.054 (20)
1.067 ± 0.074 (20)
1.079 ± 0.060 (21)
( ) = Number of cells
1.071 ± 0.007
MDA-MB-231
MDA-MB-435S
Hs578T

Table 8. Fractal dimension values of individual cells of each cell line.

	MCF10A	MCF7	T47D	ZR-75-1	MDA-MB-231	MDA-MB-435S	Hs578T
1	1.438	1.029	1.100	1.062	1.066	1.110	1.160
2	1.238	1.180	1.103	1.078	1.166	1.121	0.936
3	1.410	1.170	0.927	1.065	1.152	1.169	1.190
4	1.321	1.252	0.946	1.098	1.042	1.068	1.141
5	1.269	1.180	1.078	1.130	0.920	1.116	1.121
6	1.345	1.092	1.150	1.114	1.068	1.204	1.154
7	1.367	1.134	1.110	1.234	1.145	0.978	1.013
8	1.301	1.079	1.065	1.258	1.049	1.072	1.054
9	1.486	1.069	1.047	1.152	1.056	1.109	1.071
10	1.408	0.929	1.074	1.217	1.077	1.064	1.014
11	1.330	1.149	1.107	1.238	1.070	1.032	1.042
12	1.445	1.098	1.208	1.087	1.031	0.937	1.084
13	1.348	1.115	0.937	1.097	1.078	0.999	1.096
14	1.330	1.119	1.245	1.095	1.095	1.144	1.068
15	1.313	1.160	1.079	1.149	1.103	1.000	1.115
16	1.241	1.070	1.237	1.130	1.060	0.936	1.102
17	1.231	1.175	1.197	1.240	1.080	0.999	0.999
18	1.382	1.107	1.196	1.124	1.052	1.092	1.109
19	1.395	1.102	-	1.053	1.002	1.112	1.051
20	1.421	-	-	1.159	1.028	1.070	1.054
21	1.283	-	-	1.067	-	-	1.094
22	-	-	-	1.179	-	-	-
Mean	1.348	1.116	1.100	1.138	1.067	1.067	1.079
SD	0.073	0.069	0.097	0.065	0.054	0.074	0.060

3.8. Comparison of fractal dimension between normal, weakly and highly invasive cancer cells using optical imaging

The results show that the more ruggedness of the border, the higher fractal dimension value. It is also clear that there is difference between normal cells, weakly invasive cancer cells and highly invasive cancer cells (Fig. 9). Similar to AFM imaging results, the high resolution images of normal cell show more complexity in membranes and have higher fractal dimension value (FD = 1.348), while weakly and highly invasive cancer cell membranes show less branching and have lower fractal dimension values.

To deeply access this difference, statistical analysis was processed of these data. Using ANOVA analysis, the fractal dimension values were compared within and between groups. The analysis resulted in no significant difference within each groups and proved that there is a statistically significant difference in the average FD value between normal and cancer cells (Fig. 9B), and more important between the weakly and highly invasive cancer cell groups (Table 9) with $p < 0.05$.

In summary, optical imaging is a helpful technique to analyze fractal dimension of many cells at same time. The differences between cell lines are not only evidenced in images, but also in mathematical value calculated from fractal analysis. So fractal analysis of cell morphology may provide new way to distinguish cancer cell metastasis progression.

Figure 9. Comparison between normal, weakly invasive and highly invasive cancer cells using optical imaging. (A) The optical imaging shows differences of cell membrane morphology. Scale bar, 5 μm. The normal cell membrane (MCF10A) shows the most profuseness of branching. This gradually decreases in weakly invasive and highly invasive cancer cell morphology. (B) Comparison of fractal dimension values between different cell groups. Data were expressed as the mean ± SD values. There are statistically significant differences between normal cells and cancer cells, especially between weakly invasive and highly invasive cancer cell groups ($\star p < 0.05$, $\star\star p < 0.001$).

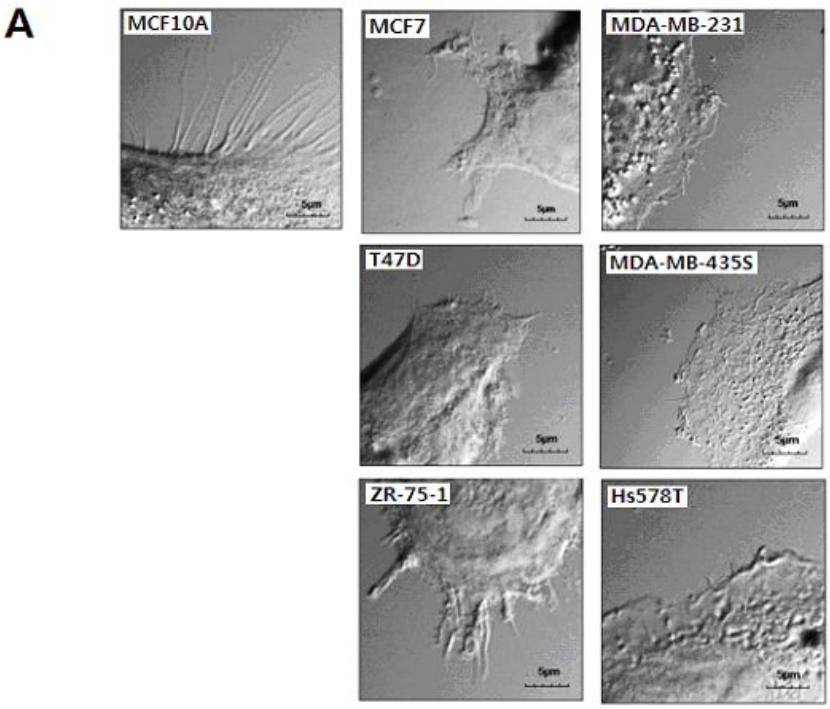
A
MCF10A
MCF7
MDA-MB-231
T47D
MDA-MB-435S
ZR-75-1
Hs578T
5μm

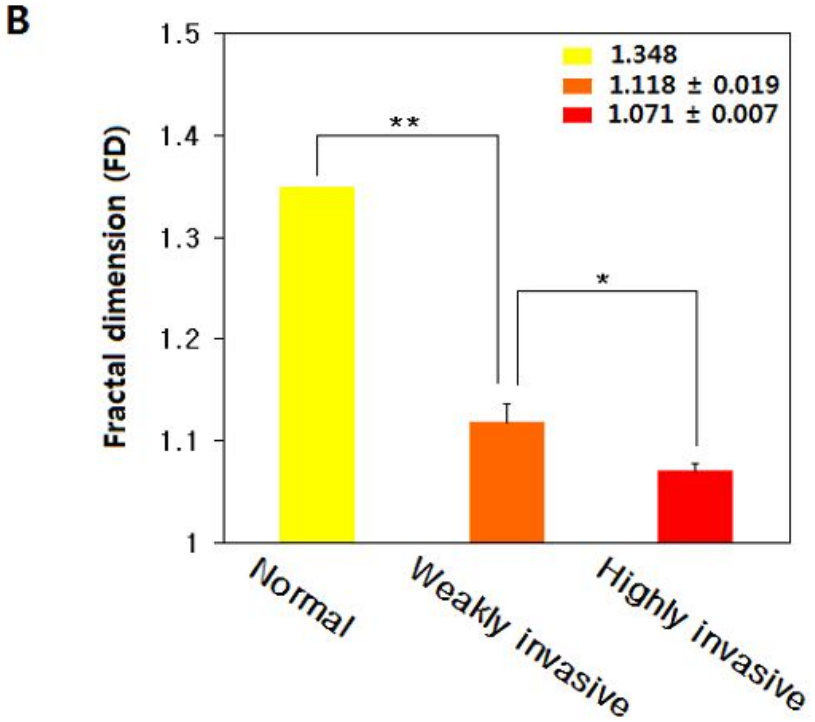
B
Fractal dimension (FD)
1.5
1.4
1.3
1.2
1.1
1
1.348
1.118 ± 0.019
1.071 ± 0.007
**
*
Normal
Weakly invasive
Highly invasive

Table 9. Fractal dimension values of weakly and highly invasive cancer cells.

	Weakly invasive cancer cells	Highly invasive cancer cells
1	1.116	1.067
2	1.100	1.067
3	1.138	1.079
Mean	1.118	1.071
SD	0.019	0.007

Chapter 4: Discussion and Conclusion

Fractal analysis recently has increasing applications in physiology, medicine, and pathology (Luzi *et al.*, 1999) but in cancer research, its advances focus on tumor border and nuclear complexity. It seems that fractal dimension of cellular morphology in cancer are still not well understood. Therefore, application of fractal analysis of cell morphology in cancer research is really a wide and interesting field. But cellular morphology exhibits self-similarity and can be access by fractal analysis (Rigaut *et al.*, 1998). This study reported initial results about fractal analysis of cancer cell morphology and the correlation of these measures with the disease stage. Hopefully, fractal methods may someday have significant impact on our understanding of challenges in treatment delivery and diagnosis of cancer.

In this current study, fractals usage focused at the cellular level. However, the results only reflect characteristics of cells in culture with laboratory conditions. If fractal dimension can be analyzed with the cells obtained directly from biopsies of cancer patients, it may give more practical information which can be applied in surgical treatments or clinical purposes. It can be seen that some research were processed directly with patients, for example pancreatic cancer (Vasilescu *et al.*, 2012). If the study is extended in the near future, fractal method is expected to be readily applicable for cancer detection.

This finding used box-counting method to calculate fractal dimension value from images of cell boundary. Private software was developed to calculate FD value.

It is really convenient and helps to save time when automatically obtaining FD value from the linear slope between the log of occupied box number and log of box size. Recently, some scientists tried to develop software to eliminate the noise from image and applied it to calculate fractal dimension value of cells from culture (Timbó *et al.*, 2009).

Cell membranes are involved in a variety of cellular processes such as cell adhesion, ion conductivity, cell signaling and serve as the attachment surface for several extracellular structures. This study focused on fractal property of cell morphology and cancer, but fractal dimensions of biological cells and tissues are also useful morphological tool for establishing the links between structure and function. Some other researchers were interested in vesicular patterning resulting from endocytic membrane activity (Krasowska *et al.*, 2009), other study shows that fractal dimension correlates well with the specific membrane dielectrics capacitance (Wang *et al.*, 2010).

The DIC images show that there is difference between the membrane structure of normal cells, weakly invasive cancer cells and highly invasive cancer cells, especially the gland-like structures of cell membrane and consequently there is difference about fractal dimension values. So it drives us for more understanding about the molecular mechanism of cell membrane. Obviously, most of cell surface extensions are based on actin filaments and the ruggedness of the plasma membrane is mainly affected by the two distinct actin-based membrane protrusions,

filopodia and lamellipodia (Abraham *et al.*, 1999). But the optical imaging cannot provide actin filament dynamic, it needs to be considered other methods or higher imaging techniques to elucidate the role of actin in cell membrane protrusion. In this study, the highly invasive cancer cells show smooth membrane than weakly invasive cancer cells. Interestingly, it seems that proteins of actin skeleton may play an important role in metastasis progression of cancer cells. Normal cells in an adult epithelium do not usually need to migrate extensively and have relatively quite cytoskeletons (Machesky, 2008). But how the body responds to cancer and how the cancer changes the body responses are extremely complex and fascinating areas of research. Furthermore, when micrometastasis are established, they typically revert toward the phenotype of original tumor and adapt to their new environment.

In conclusion, this finding investigated the fractal property of breast cancer cell morphology and calculated fractal dimension value using box-counting method. It gave the first evidence that fractal dimension changed through invasiveness stage of cancer cells. Expectedly, in the near future, fractal dimension is really useful tool for cancer diagnosis and treatment.

Chapter 5: References

Abraham, V. C.; Krishnamurthi, V.; Taylor, D. L. and Lanni, F. (1999). The actin-based nanomachine at the leading edge of migrating cells. *Biophys J* 77: 1721-32.

Ahammera, H. (2001). Fractal dimension for a cancer invasion model. *Fractals* 9: 61-76

Ahammera, H. (2008). Fractal dimension of the choriocarcinoma cell invasion front. *Physica D* 237: 446-453

Baish, J. W. and Jain, R. K. (2000). Fractals and cancer. *Cancer Res* 60: 3683-8.

Bernard, F.; Bossu, J. L. and Gaillard, S. (2001). Identification of living oligodendrocyte developmental stages by fractal analysis of cell morphology. *J Neurosci Res* 65: 439-45.

Boser, S. R.; Park, H.; Perry, S. F.; Menache, M. G. and Green, F. H. (2005). Fractal geometry of airway remodeling in human asthma. *Am J Respir Crit Care Med* 172: 817-23.

Cross, S. S. (1997). Fractals in pathology. *J Pathol* 182: 1-8.

Di Giovanni, P.; Ahearn, T. S.; Semple, S. I.; Lovell, L. M.; Miller, I.; Gilbert, F. J.; Redpath, T. W.; Heys, S. D. and Staff, R. T. (2012). The biological correlates of macroscopic breast tumour structure measured using fractal analysis in patients undergoing neoadjuvant chemotherapy. *Breast Cancer Res Treat* 133: 1199-206.

Goutzanis, L.; Papadogeorgakis, N.; Pavlopoulos, P. M.; Katti, K.; Petsinis, V.; Plochoras, I.; Pantelidaki, C.; Kavantzas, N.; Patsouris, E. and Alexandridis, C. (2008). Nuclear fractal dimension as a prognostic factor in oral squamous cell carcinoma. *Oral Oncol* 44: 345-53.

Heymans, O.; Blacher, S.; Brouers, F. and Pierard, G. E. (1999). Fractal quantification of the microvasculature heterogeneity in cutaneous melanoma. *Dermatology* 198: 212-7.

Karperien, A.; Ahammer, H. and Jelinek, H. F. (2013). Quantitating the subtleties of microglial morphology with fractal analysis. *Front Cell Neurosci* 7: 3.

Krasowska, M.; Grzywna, Z. J.; Mycielska, M. E. and Djamgoz, M. B. (2009). Fractal analysis and ionic dependence of endocytotic membrane activity of human breast cancer cells. *Eur Biophys J* 38: 1115-25.

Landini, G. and Rippin, J. W. (1996). How important is tumour shape? Quantification of the epithelial-connective tissue interface in oral lesions using local connected fractal dimension analysis. *J Pathol* 179: 210-7.

Lebedev, D. V.; Filatov, M. V.; Kuklin, A. I.; Islamov, A.; Kentzinger, E.; Pantina, R.; Toperverg, B. P. and Isaev-Ivanov, V. V. (2005). Fractal nature of chromatin organization in interphase chicken erythrocyte nuclei: DNA structure exhibits biphasic fractal properties. *FEBS Lett* 579: 1465-8.

Liu, J. Z.; Zhang, L. D. and Yue, G. H. (2003). Fractal dimension in human cerebellum measured by magnetic resonance imaging. *Biophys J* 85: 4041-6.

Losa, G. A.; Graber, R.; Baumann, G. and Nonnenmacher, T. F. (1998). Steroid hormones modify nuclear heterochromatin structure and plasma membrane enzyme of MCF-7 cells. A combined fractal, electron microscopical and enzymatic analysis. *Eur J Histochem* 42: 21-9.

Luzi, P.; Bianciardi, G.; Miracco, C.; De Santi, M. M.; Del Vecchio, M. T.; Alia, L. and Tosi, P. (1999). Fractal analysis in human pathology. *Ann N Y Acad Sci* 879: 255-7.

Machesky, L. M. (2008). Lamellipodia and filopodia in metastasis and invasion. *FEBS Lett* 582: 2102-11.

Mandelbrot, B. (1967). How long is the coast of britain? Statistical self-similarity and fractional dimension. *Science.* 156: 636-8.

Mandelbrot, B. The fractal geometry of nature. W.H. Freeman & Company. New York (1982)

Masters, B. R. (2004). Fractal analysis of the vascular tree in the human retina. *Annu Rev Biomed Eng* 6: 427-52.

Mattila, P. K. and Lappalainen, P. (2008). Filopodia: molecular architecture and cellular functions. *Nat Rev Mol Cell Biol* 9: 446-54.

Omori, H.; Nio, Y.; Yano, S.; Itakura, M.; Koike, M.; Toga, T. and Matsuura, S. (2002). A fractal dimension analysis: a new method for evaluating the response of anticancer therapy. *Anticancer Res* 22: 2347-54.

Rigaut, J. P.; Schoevaert-Brossault, D.; Downs, A. M. and Landini, G. (1998). Asymptotic fractals in the context of grey-scale images. *J Microsc* 189: 57-63.

Sedivy, R.; Windischberger, C.; Svozil, K.; Moser, E. and Breitenecker, G. (1999). Fractal analysis: an objective method for identifying atypical nuclei in dysplastic lesions of the cervix uteri. *Gynecol Oncol* 75: 78-83.

Smith, T. G., Jr.; Lange, G. D. and Marks, W. B. (1996). Fractal methods and results in cellular morphology--dimensions, lacunarity and multifractals. *J Neurosci Methods* 69: 123-36.

Song, C.; Havlin, S. and Makse, H. A. (2005). Self-similarity of complex networks. *Nature* 433: 392-5.

Spillman, W. B., Jr.; Robertson, J. L.; Huckle, W. R.; Govindan, B. S. and Meissner, K. E. (2004). Complexity, fractals, disease time, and cancer. *Phys Rev E Stat Nonlin Soft Matter Phys* 70: 061911.

Timbó, C.; da Rosa, L. A. R.; Gonçalves, M. and Duarte, S. B. (2009). Computational cancer cells identification by fractal dimension analysis. *Computer Physics Communications* 180: 850-853.

Vasilescu, C.; Giza, D. E.; Petrisor, P.; Dobrescu, R.; Popescu, I. and Herlea, V. (2012). Morphometrical differences between resectable and non-resectable pancreatic cancer: a fractal analysis. *Hepatogastroenterology* 59: 284-8.

Vilela, M. J.; Martins, M. L. and Boschetti, S. R. (1995). Fractal patterns for cells in culture. *J Pathol* 177: 103-7.

Wang, X.; Becker, F. F. and Gascoyne, P. R. (2010). The fractal dimension of cell membrane correlates with its capacitance: a new fractal single-shell model. *Chaos* 20: 043133.

ACKNOWLEDGMENT

I would like to express my special thanks to Prof. Kun Ho Lee for advising me in study and guiding me in the entire period of my Master course. I would like to express my thanks to my Lab Members: Pyung Sik Park, Merlin Jayalal Lawrence, Balaji Kannappan , Minji Kim, Nahyeon Kim, Jisu Lee for helping me in this project. I would like to express my thanks to members of Cellular and Molecular Biology Lab of Chung-Ang University and Cell Dynamics and Imaging Lab of Gwangju Institute of Science and Technology for helping me in this study. I would like to express my thanks to all of my Korean friends and Korean people for making me feel home in Korea. I would like to express my heartfelt thanks to my family and Vietnamese friends for encouraging me during my study.